Tumour growth control: analysis of alternative approaches☆

Federico Papa [a,1], Alessandro Borri [b,c,*,1], Pasquale Palumbo [d,a]

[a] *CNR-IASI, National Research Council of Italy, Via dei Taurini 19, Rome, Italy*
[b] *CNR-IASI Biomathematics Laboratory, National Research Council of Italy, L.go A. Gemelli 8, Rome, Italy*
[c] *Center of Excellence for Research DEWS, University of L'Aquila, Via Vetoio, L'Aquila, Italy*
[d] *Department of Biotechnology and Biosciences, University of Milano-Bicocca, Piazza della Scienza 2, 20126 Milan, Italy*

ARTICLE INFO

ABSTRACT

In this work we address the problem of tumour growth control by properly exploiting a low-dimensional model that grounds on the Chemical Reaction Network (CRN) formalism. Originally conceived to work both in deterministic and stochastic frameworks, it is shown that, except for the case of very low number of tumour cells, the deterministic approach is appropriate to characterize the system behaviour, especially for control planning purposes. Two alternative control approaches are here investigated. One trivially assumes a constant infusion of external drug administration, the other is designed according to a state-feedback control scheme, with complete or partial knowledge of the state. Pros and cons of both control laws are investigated, showing that the tumour size at the beginning of the therapy plays a role of paramount importance for fixed infusion therapies, whilst only state-feedback laws can eradicate arbitrarily large tumours.

1. Introduction

Model-based control is gaining an increasing interest in the last decades, since it allows the design of very sophisticated feedback regulations accounting for the innate dynamics of the system under investigation. Within biomedical frameworks, minimal models are often exploited since they allow to catch the basic relationships among the involved variables without explicitly detailing all the physical/molecular mechanisms: they can be easily identified according to standard perturbation experiments, and allow the synthesis of affordable and readily implementable control laws.

As far as tumour growth models are concerned, starting from the seminal paper (Hahnfeldt et al., 1999) (proposing an Ordinary Differential Equation (ODE) model of the vascular growth of tumours characterized by low dimension and minimal number of parameters) several theoretical/experimental results have been achieved, dealing with model extensions (see d'Onofrio and Gandolfi, 2004, 2010) and closed-/open-loop anti-angiogenic drugging (see, e.g. Cacace et al., 2018b,a; Drexler et al., 2017c; Ledzewicz and Schättler, 2008; Sápi et al., 2016), possibly combined with chemotherapy treatments (see, e.g. d'Onofrio et al., 2009; Ledzewicz et al., 2011). Feedback controls of tumour growth kinetic models have been also proposed in stochastic frameworks, like the recent contributions Preziosi et al. (2021) and

Medaglia et al. (2022) exploiting mathematical tools from statistical physics. The theoretical approaches aiming at providing tumour dynamics characterization are very frequent (see e.g. Pinho et al., 2013), even in the context of more complex age/spatial-structured PDE models (see e.g. Liu et al., 2019; Wei and Cui, 2008). Such a kind of mathematical analysis allows to identify conditions for carcinogenesis and for tumour growth and invasion, which are fundamental results for tumour control planning and for optimizing treatments (see Dzyubak et al., 2019).

More recently, models of tumour growth have been proposed (Drexler et al., 2019, 2017a,b) as coming from the formalism of Chemical Reaction Network (CRN) (Feinberg, 2019). The advantage of such an approach is that CRN can be straightforwardly modelled according to the stochastic framework implemented by the Chemical Master Equations (CME) (Borri et al., 2020), able to account for the inherent noise providing random fluctuations on the involved chemical players; the usual (ODE) models associated to CRNs may be thought of as a linear approximation of the average dynamics coming from the CME (van Kampen, 2007). These ODE models can be fruitfully exploited in spite of the more complete CMEs whenever the chemical players copy number is very high, because of their superior computational manageability. In this work it is shown by realistic numerical simulations that

the stochastic approach may be set aside for tumour growth control purposes, at least at the beginning of an exogenous drug administration therapy, because such therapies are supposed to start with a very large number of tumour cells. Instead, assuming to have successfully reduced the initial tumour mass, it could be interesting to approach the tumour eradication problem from a stochastic control perspective, dealing with a very low number of leftover tumour cells.

In fact, this contribution starts from the qualitative analysis carried out in Borri et al. (2020) for the ODE model associated to the CRN and further investigates tumour growth control techniques accounting for both fixed and state-dependent feedback control laws. The main results of this paper show that constant administration therapies have several limitations. In particular, they cannot eradicate the tumour if its size is too large when the therapy starts. Conversely, a state-feedback control law can overcome the limitations of the constant therapy. Indeed, it is always possible to design a control scheme able to eradicate arbitrarily large tumours, allowing a high infusion rate only for a limited time period.
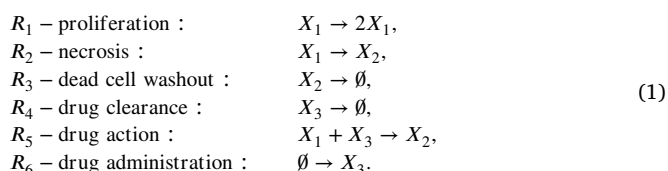
The next Section is devoted to briefly recap the equations and the main features of the model. It will be shown that the stochastic approach provides a significant contribution only according to very low copy numbers: although interesting when dealing with the issue of complete tumour eradication, such an approach will not be kept in the sequel, in favour of an in-depth investigation of tumour size control in the deterministic model, which provides a good approximation of the mean behaviour of the stochastic one. Section 3 deals with the case of a fixed drug administration; it will be shown how the initial tumour size is responsible of a successful tumour eradication and how we can cope with adverse initial conditions. Section 4 gets in the details of state-feedback control, showing that only such a control scheme can eradicate arbitrarily large tumours. Conclusions follow. Finally, an Appendix reporting some details on the (both deterministic and stochastic) adopted numerical strategies closes the paper.

2. Model formulation: deterministic vs stochastic approach

In the recent paper (Borri et al., 2020) we provided a double formulation, deterministic versus stochastic, of a growing tumour cell population under chemotherapeutic treatment. The proposed deterministic–stochastic model is a minimally parameterized and low-dimensional system taking into account the dynamics of proliferating and dead cancer cells, as well as the anti-cancer drug level. Our modelling framework generalizes the approach introduced by Drexler et al. (2019), where the well known CRN formalism (see Feinberg, 2019 for the details) is exploited for describing physiological aspects and cell-drug interaction, and it allows to derive an ODE system describing the dynamics of the treated tumour.

The deterministic formulation describes the system behaviour in average terms, as it actually well approximates the first moment of the stochastic representation. Nevertheless, a stochastic formulation is mandatory in order to provide a more realistic representation of the system, characterized by random fluctuations and correlations between state variables (see van Kampen, 2007).

As described in Borri et al. (2020), the chemical players considered by the stochastic formulation are: (i) growing cancer cells, X_1, (ii) necrotic cancer cells, X_2, and (iii) drug molecules, X_3; moreover, the physiological aspects and the state interactions that have been represented are:

$$
\begin{aligned}
R_1 &- \text{proliferation}: & X_1 &\rightarrow 2X_1, \\
R_2 &- \text{necrosis}: & X_1 &\rightarrow X_2, \\
R_3 &- \text{dead cell washout}: & X_2 &\rightarrow \emptyset, \\
R_4 &- \text{drug clearance}: & X_3 &\rightarrow \emptyset, \\
R_5 &- \text{drug action}: & X_1 + X_3 &\rightarrow X_2, \\
R_6 &- \text{drug administration}: & \emptyset &\rightarrow X_3.
\end{aligned}
\tag{1}
$$

Following the usual stochastic approach, we opted for countable variables n_i, $i = 1, 2, 3$, (number of cancer cells and drug molecules) to

Table 1
Population resets according to the set of reactions (1).

Event	Resets	propensities
R_1	$n_1 \mapsto n_1 + 1$	$a_1 = k_1 n_1$
R_2	$\begin{cases} n_1 \mapsto n_1 - 1 \\ n_2 \mapsto n_2 + 1 \end{cases}$	$a_2 = k_2 n_1$
R_3	$n_2 \mapsto n_2 - 1$	$a_3 = k_3 n_2$
R_4	$n_3 \mapsto n_3 - 1$	$a_4 = \rho \frac{n_3}{M_4 + n_3}$
R_5	$\begin{cases} n_1 \mapsto n_1 - 1 \\ n_2 \mapsto n_2 + 1 \\ n_3 \mapsto n_3 - 1 \end{cases}$	$a_5 = k_5 \frac{n_1 n_3}{M_5 + n_3}$
R_6	$n_3 \mapsto n_3 + 1$	$a_6 = r$

denote the values of the chemicals X_i. When a reaction in (1) occurs, the state $n = (n_1, n_2, n_3)$ updates according to the resets of Table 1. The third column in 1 refers to the propensities a_i, $i = 1, \ldots, 6$, related to the probabilities of occurrence of reactions R_i in $(t, t + dt)$ (namely $a_i dt$, see Borri et al., 2020).

Besides, according to the usual mathematical formalism, coefficients k_i, $i = 1, 2, 3, 5$, in Table 1 are the reaction rate constants (day^{-1}) of reactions R_i, $i = 1, 2, 3, 5$, M_i, $i = 4, 5$, are the MM constants (number of cells/molecules) of reactions R_i, $i = 4, 5$, ρ is the maximal rate of drug elimination (molecules per day) of reaction R_4 and r is the treatment rate (molecules per day) of reaction R_6. Note that, in principle, r can be time-varying and dependent on the drugging regimen.

According to Table 1, the stochastic model of system (1) is given by the Chemical Master Equations (CME) describing the dynamics of the grand probability function $P(\eta_1, \eta_2, \eta_3; t)$, that is the probability that the state $n(t)$ is equal to the value $\eta = (\eta_1, \eta_2, \eta_3)^T$ at time t. In particular, denoting by $\delta_i \in \mathbb{R}^3$ the vector of resets referred to the state (n_1, n_2, n_3) because of reaction R_i, the CME (Borri et al., 2020; van Kampen, 2007; Borri et al., 2016) is written as

$$
\partial P(\eta; t) / \partial t = \sum_{i=1}^{6} \left[a_i(\eta - \delta_i) P(\eta - \delta_i; t) - a_i(\eta) P(\eta; t) \right].
\tag{2}
$$

Fig. 1 shows the state transition maps for any reaction occurrence providing a transition *from* state (η_1, η_2, η_3) (upper panel of Fig. 1, negative terms in Eq. (2)) and any reaction occurrence providing a transition *into* state (η_1, η_2, η_3) (lower panel of Fig. 1, positive terms in Eq. (2)).

As it usually happens, CME cannot be directly solved because of the combinatorial explosion of the possible state values: dealing with millions of cancer cells, necrotic cells and drug molecules would lead to $(10^6)^3 = 10^{18}$ distinct states η, each described by a CME of the type (2). Such a curse of dimensionality prevents the search for analytical solutions, even according to recent computational schemes relying on efficient state-space realization of the CME, Borri et al. (2016). In these cases, one may resort to search for a less informative model, looking for first-order (or higher-order) moment equations. Unfortunately, because of the nonlinearity fashion of some model propensities, moment equations are not achievable in closed form van Kampen (2007). The application of a linear approximation to first-order moments provides the usual ODE equations coming out when the chemical reaction network is directly translated into a kinetic compartmental model, following the classical deterministic modelling approach based on the stoichiometry matrix definition (where the reset vector δ_i previously introduced coincides with the ith column of the stoichiometry matrix van Kampen, 2007). Denoting by $\langle n_i \rangle$, $i = 1, 2, 3$, the average values of n, the ODE system approximately describing the
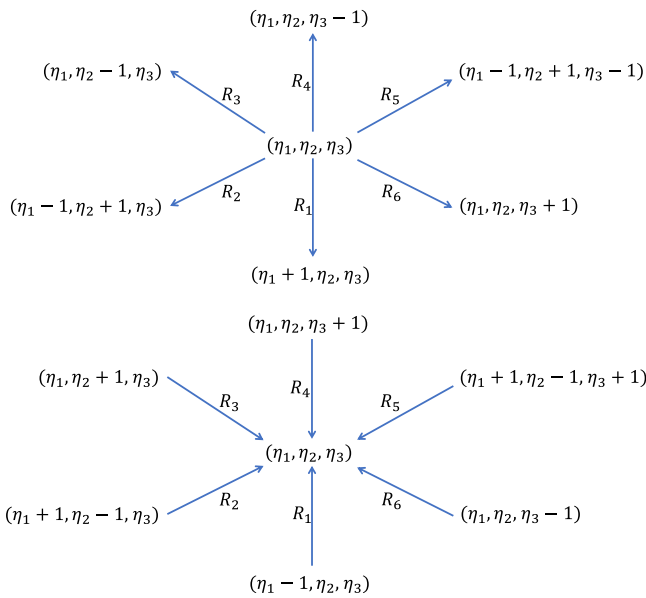
Fig. 1. State transition diagram for the CME (2).

average values is given by

$$
\begin{aligned}
\frac{d\langle n_1\rangle}{dt} &= (k_1 - k_2)\langle n_1\rangle - k_5 \frac{\langle n_1\rangle\langle n_3\rangle}{M_5 + \langle n_3\rangle}, \\
\frac{d\langle n_2\rangle}{dt} &= k_2\langle n_1\rangle - k_3\langle n_2\rangle + k_5 \frac{\langle n_1\rangle\langle n_3\rangle}{M_5 + \langle n_3\rangle}, \\
\frac{d\langle n_3\rangle}{dt} &= -\rho\frac{\langle n_3\rangle}{M_4 + \langle n_3\rangle} - k_5 \frac{\langle n_1\rangle\langle n_3\rangle}{M_5 + \langle n_3\rangle} + r.
\end{aligned}
\tag{3}
$$

Notice that the deterministic model can well approximate the mean value of the Markov chain provided that the drug copy number n_3 is far from the saturation values of the MM functions (achieved when $n_3 \gg M_4, M_5$), which makes the MM propensity functions close to be linear.

In summary, starting from the more complete stochastic formulation, the standard ODE deterministic model is derived as the first-order approximation of the CME average values and it is usually preferred to the CME model when the copy number of the involved species is high enough to average and smooth the relative fluctuations. Dealing with a model of tumour growth there may not be a clear separation between the two cases (i.e. high copy number versus low copy number), and both approaches may well deserve a thorough analysis, especially when a tumour growth control law is applied: at the beginning of the delivered drug therapy it is reasonable to assume a very high copy number of tumour cells, so that the ODE may be preferable to lighten the computational burden; on the other hand, in case of a successful drug therapy, tumour cells may reduce to such a low level to make more reasonable to account for the stochastic approach.

To better investigate what happens to the case at hand, we have simulated different scenarios according to the τ-leap algorithm Gillespie (2001): this method has been preferred to standard Gillespie algorithm (providing statistically exact simulations) Gillespie (1976) because the very high cell copy number entailed impractically long simulations. Figs. 2 and 3 report some numerical simulations obtained by means of the stochastic modelling approach and its deterministic ODE approximation.

Parameters are reported in Table 2 and are set according to experimental values related to Pegylated Liposomal Doxorubicin treatment and breast cancer cells of mice (see Borri et al., 2020 for details). Under suitable hypotheses, described in Section 3, the drugging rate r is kept constant and equal to the same value, i.e. $1.53 \cdot 10^9$ drug molecules per day, picked in the interval $(\beta\rho, \rho)$, where the parameter function β is

Table 2
Values of the model parameters for the deterministic model. The model-dependent quantities β and n_{10}^{max} are computed from Eqs. (6) and (17).

Parameter	Value
k_1	$exp(-1.18)$
k_2	$exp(-1.94)$
k_3	$exp(-1.08)$
k_5	$exp(-1.79)$
M_4	$5.553 \cdot 10^{10}$
M_5	$1.495 \cdot 10^{7}$
ρ	$3.953 \cdot 10^{10}$
β	0.0128
n_{10}^{max}	$2.386 \cdot 10^{11}$

given by Eq. (6). A unique and asymptotically stable equilibrium point is ensured by the chosen model parameters and by the constant rate of drug administration.

The random paths reported in Fig. 2 are obtained starting from the initial state $(n_1(0), n_2(0), n_3(0)) = (3.95 \cdot 10^6, 100, 0)$. It can be appreciated that the deterministic behaviour very well resembles the first moment dynamics and that, according to the chosen parameter values, the high number of tumour cells makes the stochastic fluctuations actually negligible. Conversely, assuming a different initial scenario characterized by a reduced copy number of proliferating cells (initial growth phase), noise fluctuations become significant. Fig. 3 shows the comparison between the stochastic model and the deterministic one when $(n_1(0), n_2(0), n_3(0)) = (300, 100, 0)$. It can be noted from the figure that, although the mean trend of the random path is still well captured by the deterministic model, now the fluctuations actually are highly appreciable. Moreover, the random fluctuations allow the tumour to reach a maximal dimension that is almost double with respect to the maximal value reached by the mean trend.

It is worth noticing that the case of very few cell copies is of interest for the stochastic formulation when dealing with tumour eradication strategies, that is when the planning of a suitable control law is crucial to bring n_1 to zero. Nevertheless, the design of a stochastic control is not the aim of the present work, but it is a future development naturally arising from the present results. In this paper we further investigate the qualitative behaviour of the first moment approximation of the stochastic model, that is the dynamical system (3), and possible related control strategies addressing tumour eradication (at least on average).

In the following Section, the state variables of the ODE in (3) will be shortly denoted by n_i rather than $\langle n_i\rangle$.

3. Model dynamics under a fixed infusion therapy

As a first remark, we highlight that all the reaction rates in the ODE model (3) are bounded and continuously-differentiable (hence Lipschitz-continuous) in the positive orthant, which is a sufficient condition for the existence and uniqueness of the solution of the model, as well as for the search of the equilibrium points of the ODE unique solution as the roots of the algebraic equation coming from setting $\frac{d\langle n_i\rangle}{dt} = 0$, $i = 1, 2, 3$ in (3), see e.g. Khalil (1996). With regards to the qualitative behaviour of the ODE model (3) under a fixed infusion $r(t) = \bar{r}$, in Borri et al. (2020) we proved the existence and stability properties of the equilibrium points summarized by Table 3, where

$$
E_1 = \left(0, 0, M_4\frac{\bar{r}}{\rho - \bar{r}}\right),
\tag{4}
$$

and

$$
E_2 = \left(\frac{\bar{r} - \beta\rho}{k_1 - k_2}, \frac{k_1}{k_3}\frac{\bar{r} - \beta\rho}{k_1 - k_2}, \frac{M_5(k_1 - k_2)}{k_5 - k_1 + k_2}\right),
\tag{5}
$$

with

$$
\beta = M_5(k_1 - k_2)/(M_4(k_5 - k_1 + k_2) + M_5(k_1 - k_2)),
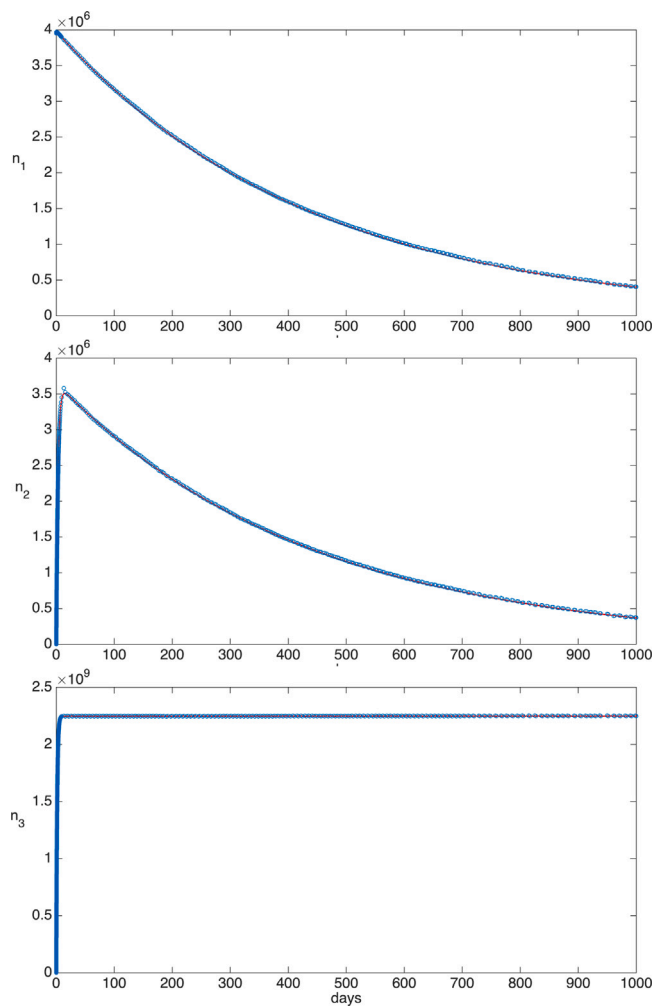\tag{6}
$$

Fig. 2. Random paths from τ-leap stochastic simulations (blue dots) overlapping the approximate first-order dynamics (red line) when $(n_1(0), n_2(0), n_3(0)) = (3.95 \cdot 10^6, 100, 0)$. Parameters are taken from Table 2. Constant administration rate r fixed to $1.53 \cdot 10^9$ drug molecules per day.

Fig. 3. Random paths from τ-leap stochastic simulations (blue dots) and the approximate first-order dynamics (red line) for $(n_1(0), n_2(0), n_3(0)) = (300, 100, 0)$. Parameters are taken from Table 2. Constant administration rate r fixed to $1.53 \cdot 10^9$ drug molecules per day.

Table 3
Existence and stability of the equilibrium points of system (3). $f = \{(\xi, \frac{k_1}{k_3}\xi, 0) : \xi \geq 0\}$ is a family of points existing only in the limit condition $k_1 = k_2$, $\bar{r} = 0$.

Parameter region		Infusion rate	Equilibrium	Stability
$k_1 < k_2$		$0 \leq \bar{r} < \rho$	E_1	Locally asympt. stable
		$\bar{r} \geq \rho$	$\nexists$	–
$k_1 = k_2$		$\bar{r} = 0$	$f(\supset \{E_1\})$	Nothing can be said
		$0 < \bar{r} < \rho$	E_1	Locally asympt. stable
		$\bar{r} \geq \rho$	$\nexists$	–
$k_1 > k_2$	$k_5 \leq k_1 - k_2$	$0 \leq \bar{r} < \rho$	E_1	Unstable
		$\bar{r} \geq \rho$	$\nexists$	–
	$k_5 > k_1 - k_2$	$0 \leq \bar{r} < \beta\rho$	E_1	Unstable
		$\bar{r} = \beta\rho$	$E_1 \equiv E_2$	Nothing can be said
		$\beta\rho < \bar{r} < \rho$	E_1	Locally asympt. stable
			E_2	Unstable
		$\bar{r} \geq \rho$	E_2	Unstable

refer to two distinct equilibrium points: the former (E_1) provides tumour eradication and it can be locally asymptotically stable according to specific model parameter values (included the fixed drug administration rate); the latter (E_2) refers to a non-trivial point (with respect to the three state variables) but reveals to be unstable regardless of the model parameter setting. Therefore, only E_1 is of interest for medical applications.

By reading the table, the following points can be stressed:

– for $k_1 < k_2$ we are in the lucky case where even without any treatments (i.e. $\bar{r} = 0$) we have tumour eradication because the n_1 time derivative is negative, whatever the positive initial conditions: in case of a drug treatment lower than ρ, the tumour eradication reflects the local stability of an equilibrium point with a non-trivial stationary value for the drug accumulation (that is equal to zero for no drug administration). This is a case where no intervention is required;

– for $k_1 > k_2$ and $k_5 \leq k_1 - k_2$, if point E_1 exists, it is unstable for any value of the drug administration therapy. We are in the very unlucky case where no fixed treatment is able to change the fate of a definitely increasing tumour; this is attributable to a scarce efficacy of the chosen drug, since the maximal rate constant of cell killing is lower than the net proliferation rate constant;
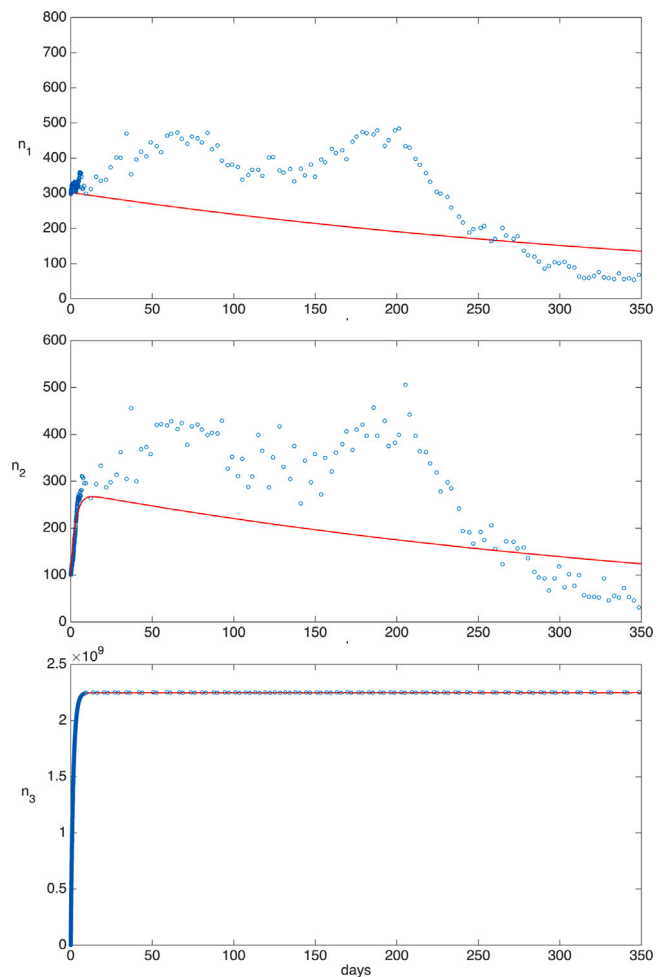
– for $k_1 > k_2$ and $k_5 > k_1 - k_2$, point E_1 is locally asymptotically stable for specific values of the exogenous drug treatment: $\beta\rho < \bar{r} < \rho$.

We stress the fact that all the properties given above are local properties (i.e. valid in a subregion of the state-space sufficiently close to the considered equilibrium point) and they are obtained for a constant administration rate. Let us now better characterize the global

dynamical properties of system (3) focusing only on the case for which it is actually reasonable to look for an effective anticancer treatment, i.e.

$$k_1 > k_2, \qquad k_5 > k_1 - k_2, \qquad \beta\rho < \bar{r} < \rho. \tag{7}$$

In the following we will prove that, under a constant administration rate $\bar{r}$ (fixed within $(\beta\rho, \rho)$), the dynamical behaviour of the state variables strongly depends on their initial values, and in particular on the tumour size when the therapy starts.

Let us restrict our analysis to the ODEs of n_1 and n_3 only, since they are totally independent of the dynamical behaviour of n_2 (n_2 does not enter in the equations of $\dot{n}_1$, $\dot{n}_3$, although it is obviously influenced by n_1, n_3). We start noticing that every real scenario begins from the initial conditions $n_1(0) = n_{10}$, with $n_{10} > 0$, and $n_3(0) = 0$. Since $\bar{r}$ is strictly positive, n_3 becomes strictly positive too as soon as we move from the initial instant $t = 0$ and it never comes back to zero. Indeed, otherwise, there would exist a time instant $\bar{t}$ such that

$$n_3(\bar{t}) = 0, \qquad \dot{n}_3(\bar{t}) \le 0$$

that is impossible. Conversely, if n_1 possibly became zero at a time $t_\star$, it would remain equal to zero because the solution should satisfy the Cauchy problem for the system (of decoupled equations)

$$\begin{cases} \dot{n}_1 = 0, \\ \dot{n}_2 = -k_3 n_2, \\ \dot{n}_3 = -\rho \dfrac{n_3}{M_4 + n_3} + r, \\ n_1(t_\star) = 0, \ n_2(t_\star) = n_{2\star}, \ n_3(t_\star) = n_{3\star}, \end{cases}$$

which, due to the uniqueness argumentation highlighted at the beginning of this Section, implies a unique solution with $n_1(t) = 0, \forall t \ge t_\star$. Moreover, when n_1 is zero the dynamics of n_3 becomes very simple, asymptotically converging to the equilibrium value of E_1, independently of its starting point (see the dynamical equation of $\dot{n}_3$ setting $n_1 = 0$).

Recalling the parameter relation $k_5 > k_1 - k_2 > 0$, it is easy to find that, as long as $n_1 \neq 0$, the following results related to $\dot{n}_1$ hold:

$$\begin{cases} \dot{n}_1 > 0 \Leftrightarrow n_3 < \bar{n}_3, \\ \dot{n}_1 = 0 \Leftrightarrow n_3 = \bar{n}_3, \\ \dot{n}_1 < 0 \Leftrightarrow n_3 > \bar{n}_3, \end{cases} \tag{8}$$

where

$$\bar{n}_3 = \frac{(k_1 - k_2)M_5}{k_5 - k_1 + k_2}. \tag{9}$$

Conversely, from the equation of $\dot{n}_3$ it is possible to find the properties

$$\begin{cases} \dot{n}_3 > 0 \Leftrightarrow n_1 < g(n_3), \\ \dot{n}_3 = 0 \Leftrightarrow n_1 = g(n_3), \\ \dot{n}_3 < 0 \Leftrightarrow n_1 > g(n_3), \end{cases} \tag{10}$$

where the function $g(n_3)$ is given by

$$g(n_3) = \frac{(\bar{r}M_4 - (\rho - \bar{r})n_3)(M_5 + n_3)}{k_5(M_4 + n_3)n_3}. \tag{11}$$

As far as the behaviour of the function (11) is concerned, denoting by $\bar{\bar{n}}_3$ the drug concentration at the equilibrium E_1, i.e. $\bar{\bar{n}}_3 = \bar{r}M_4/(\rho - \bar{r})$, the following properties hold:

$$\begin{cases} g(n_3) > 0 \Leftrightarrow n_3 < \bar{\bar{n}}_3, \\ g(n_3) = 0 \Leftrightarrow n_3 = \bar{\bar{n}}_3, \\ g(n_3) < 0 \Leftrightarrow n_3 > \bar{\bar{n}}_3, \\ \lim\limits_{n_3 \to 0} g(n_3) = \infty, \\ \lim\limits_{n_3 \to \infty} g(n_3) = -\dfrac{\rho - \bar{r}}{k_5} < 0. \end{cases} \tag{12}$$

Another important property of $g(n_3)$ can be given looking at its derivative, that is

$$\frac{dg(n_3)}{dn_3} = \frac{1}{(k_5(M_4 + n_3)n_3)^2} \Big[-(\rho - \bar{r})k_5(M_5 + n_3)(M_4 + n_3)n_3$$

$$-(\bar{r}M_4 - (\rho - \bar{r})n_3)k_5((M_4 + n_3)M_5 + n_3^2 + M_5 n_3) \Big]. \tag{13}$$

Recalling that $\bar{r}$ is strictly lower than ρ, it is easy to verify that

$$n_3 \le \bar{\bar{n}}_3 \Rightarrow \frac{dg(n_3)}{dn_3} < 0. \tag{14}$$

This property guarantees a monotonic decreasing behaviour of the function $n_1 = g(n_3)$ in the region of interest of the plane (n_3, n_1), i.e. in the non-negative orthant.

We finally provide another important property that allows to determine the relative position of the curves $\dot{n}_1 = 0$ (related to $n_1 \neq 0$) and $\dot{n}_3 = 0$ in the considered region of the state-space. In particular, we notice that the condition $\bar{r} > \beta\rho$ straightforwardly provides the following ordering of the quantities $\bar{n}_3$ and $\bar{\bar{n}}_3$:

$$\bar{r} > \beta\rho \Leftrightarrow \bar{n}_3 < \bar{\bar{n}}_3. \tag{15}$$

Fig. 4 shows a summarizing picture of all the properties given by Eqs. (8)–(15) in the non-negative orthant of the plane (n_3, n_1). Note that the state vectors $(\bar{\bar{n}}_3, 0)$ and $(\bar{n}_3, \bar{n}_1)$ are both characterized by the stationary conditions $\dot{n}_1 = 0$, $\dot{n}_3 = 0$ and they actually represent E_1 and E_2, respectively. Indeed, setting $n_3 = \bar{n}_3$ in the expression of $g(n_3)$, we obtain

$$\bar{n}_1 = g(\bar{n}_3)$$

$$= \frac{\bar{r}(M_4(k_5 - k_1 + k_2) + M_5(k_1 - k_2)) - \rho M_5(k_1 - k_2)}{(M_4(k_5 - k_1 + k_2) + M_5(k_1 - k_2))(k_1 - k_2)} = \frac{\bar{r} - \beta\rho}{k_1 - k_2}. \tag{16}$$

Based on the results given above, and depicted by Fig. 4, we are now able to provide the following theorem.

Theorem 1. *The dynamical behaviour of system (3) in the parameter region (7) is such that*

1. *if $n_3(0) \ge \bar{n}_3$, $0 \le n_1(0) \le \bar{n}_1$, and $(n_3(0), n_1(0)) \neq (\bar{n}_3, \bar{n}_1)$ (green area of Fig. 4 not including E_2) then $(n_3(t), n_1(t)) \to (\bar{\bar{n}}_3, 0)$ for $t \to \infty$;*
2. *if $0 \le n_3(0) \le \bar{n}_3$, $n_1(0) \ge \bar{n}_1$, and $(n_3(0), n_1(0)) \neq (\bar{n}_3, \bar{n}_1)$ (red area of Fig. 4 not including E_2) then $(n_3(t), n_1(t)) \to (0, \infty)$ for $t \to \infty$.*

Proof. Concerning item 1, we start by proving this property for all the internal points of the green area. Indeed, all these points are characterized by the property $\dot{n}_1 < 0$. Then, if it is guaranteed that the state trajectory does not exit from this region, then n_1 will necessarily go to zero (as it is always non-negative and it is $\dot{n}_1 = 0$ when $n_1 = 0$) when $t \to \infty$ and, consequently, n_3 will tend to $\bar{\bar{n}}_3$. The trajectory exiting from the area is actually not allowed because of the very own derivative sign of the state variables. In particular, the border $n_3 = \bar{n}_3$, $0 \le n_1 \le \bar{n}_1$ cannot be reached starting from the inside as the whole area between this border, the curve $n_1 = g(n_3)$ and the axis n_3 is characterized by the condition $\dot{n}_3 \ge 0$, which prevents n_3 to approach $\bar{n}_3$ from higher values. Moreover, the border $n_1 = \bar{n}_1$, $n_3 \ge \bar{n}_3$ cannot be reached from the inside as the whole area between this border and the curve $n_1 = g(n_3)$ is characterized by the condition $\dot{n}_1 \le 0$, which prevents n_1 to approach $\bar{n}_1$ from lower values. Finally, as previously said, the border $n_1 = 0$, $n_3 \ge \bar{n}_3$ can be reached but it cannot be crossed because of the condition $\dot{n}_1 = 0$ characterizing all its points.

We complete the proof of item 1, noting that if we start from any point of the borders except E_2, the trajectory will tend again to the limit point $(\bar{\bar{n}}_3, 0)$. Indeed, since all the points satisfying $n_3 = \bar{n}_3$, $0 < n_1 < \bar{n}_1$ and those satisfying $n_1 = \bar{n}_1$, $n_3 > \bar{n}_3$ are characterized by $\dot{n}_3 > 0$ and by $\dot{n}_1 < 0$, respectively, a state trajectory starting from any of these points will enter the green area as soon as t increases from zero, and then it will proceed as described above. Conversely, as already said, if the trajectory starts from the border $n_1 = 0$, $n_3 \ge \bar{n}_3$, n_1 does not change while n_3 goes towards $\bar{\bar{n}}_3$.

In order to prove item 2, we can follow similar arguments to those used for item 1. Let us start by proving the property for all the internal points of the red area, which are characterized by the constant property $\dot{n}_1 > 0$. If the state trajectory does not exit from this area, n_1 will
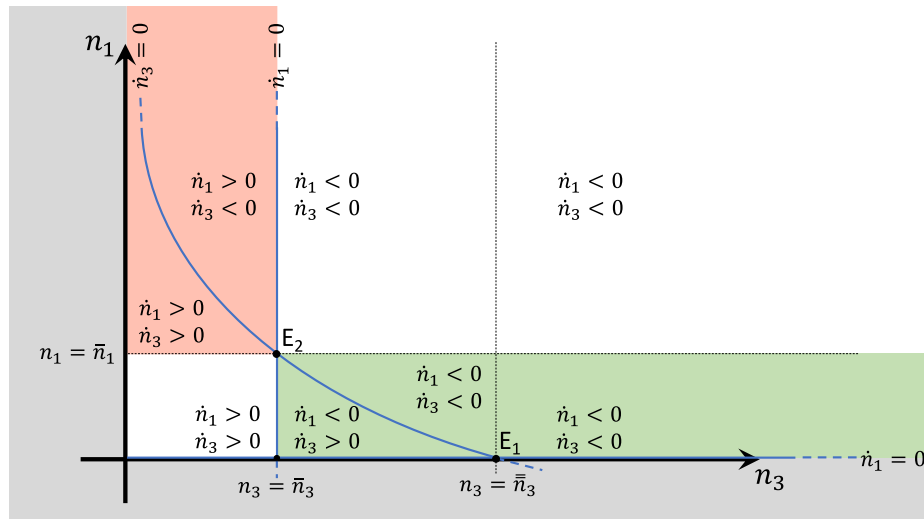
Fig. 4. Sign framework of the time derivatives $\dot{n}_1$, $\dot{n}_3$ as functions of the state in the non-negative orthant of (n_3, n_1)-plane. The solid blue line denoted by $\dot{n}_3 = 0$ represents the graph of the function $n_1 = g(n_3)$, described by Eq. (11). The critical values $\bar{n}_3$, $\bar{n}_1$ can be computed by means of Eqs. (9), (16); according to the parameter values of Table 2 and to the administration rate $\bar{r} = 1.53 \cdot 10^9$, it is $\bar{n}_3 = 7.1864 \cdot 10^8$, $\bar{n}_1 = 6.3168 \cdot 10^9$.

necessarily diverge when $t \to \infty$, while the corresponding evolution of n_3 will converge to zero. Indeed, the sign of $\dot{n}_3$ on both sides of the curve $n_1 = g(n_3)$ within the red area is such that the evolution of n_3 is always pushed towards such a curve, that actually approaches the axis $n_3 = 0$ while $t \to \infty$. We can assure again that the trajectory exiting from this area is not allowed, by looking at the derivative sign of the state variables. In particular, the border $n_3 = \bar{n}_3$, $n_1 \geq \bar{n}_1$ cannot be reached starting from the inside as the whole area between this border and the curve $n_1 = g(n_3)$ is characterized by the condition $\dot{n}_3 \leq 0$, which prevents n_3 to approach $\bar{n}_3$ from lower values. Moreover, the border $n_1 = \bar{n}_1$, $n_3 \leq \bar{n}_3$ cannot be reached from the inside as the whole area between this border, the curve $n_1 = g(n_3)$ and the axis n_1 is characterized by the condition $\dot{n}_1 \geq 0$, which prevents n_1 to approach $\bar{n}_1$ from higher values. Finally, as previously said, the border $n_3 = 0$, $n_1 \geq \bar{n}_1$ cannot be reached, at least for finite time intervals, because of the condition $\dot{n}_3 > 0$ characterizing all its points.

We complete the proof of item 2, noting that if we start from any point of the borders except E_2, the trajectory will tend again to the limit point $(0, \infty)$. Indeed, since all the points verifying $n_3 = \bar{n}_3$, $n_1 > \bar{n}_1$ and those verifying $n_1 = \bar{n}_1$, $n_3 < \bar{n}_3$ are characterized by $\dot{n}_3 < 0$ and by $\dot{n}_1 > 0$, respectively, a state trajectory starting from any of these points will enter the red area as soon as t increases from zero, and then it will proceed as described above. Conversely, as already said, if the trajectory starts from the border $n_3 = 0$, $n_1 \geq \bar{n}_1$, n_3 will increase because of the property $\dot{n}_3 = \bar{r} > 0$ and the trajectory will enter the red area (so proceeding as described above).

Taking into account the results of Theorem 1 we can now provide the following remark concerning real scenarios, which are characterized by an initial condition $(n_3(0), n_1(0))$ belonging to the axis $n_3 = 0$, $n_1 > 0$, i.e. $(n_3(0), n_1(0)) = (0, n_{10})$, with $n_{10} > 0$.

Remark 1. With reference to the parameter setting given by (7) and to a constant administration rate $\bar{r} \in (\beta\rho, \rho)$, the value n_{10} characterizing the tumour size when the therapy starts has a crucial impact on the dynamical evolution of system (3). As a matter of fact, if the administration rate were chosen without a proper evaluation of the tumour initial size the therapy could fail. In particular, if the condition $n_{10} \geq \bar{n}_1$ were satisfied the tumour would indefinitely grow, independently of the value of the constant administration rate. However, note that the

threshold $\bar{n}_1$ actually depends on $\bar{r}$ (see Eq. (16)); so, in principle, it is possible to set the value of the administration rate in order to increase $\bar{n}_1$ and to keep n_{10} far from the critical region of unlimited growth (red area of Fig. 4). Indeed, Eq. (16) shows that, when $\bar{r}$ increases, $\bar{n}_1$ increases too, and the condition $n_{10} < \bar{n}_1$ could be reached if there were no size limitations on $\bar{r}$. Nevertheless, the constraint $\bar{r} < \rho$ (hindering the unlimited drug accumulation of a constant therapy) can prevent the therapy planning from reaching the desired condition $n_{10} < \bar{n}_1$. In other words, if the initial tumour size is such that $n_{10} \geq n_{10}^{max}$, where

$$n_{10}^{max} = \frac{(1 - \beta)\rho}{k_1 - k_2}, \tag{17}$$

there is no constant administration rate which satisfies both the upper bound $\bar{r} < \rho$ and the condition $n_{10} < \bar{n}_1$.

Although setting $\bar{r}$ such that $n_{10} < \bar{n}_1$ is necessary to avoid a certain therapy failure, such a condition does not guarantee the tumour eradication, that is the convergence of the system dynamics to the equilibrium E_1. It is evident from the results of Theorem 1, as well as from Fig. 4, that the outcome of a constant therapy s.t. $0 < n_{10} < \bar{n}_1$ strongly depends on the rapidity of growth that characterizes both n_1 and n_3 during the initial phase of their evolution. Indeed, $\dot{n}_1$ and $\dot{n}_3$ are both strictly positive until $n_1 < \bar{n}_1$ and $n_3 < \bar{n}_3$ and, sooner or later, one out of the two upper bounds will be reached by the state trajectory. Then, the final outcome actually depends on which variable reaches its critical value before the other one. Let us denote by $(0, \bar{t})$, with $\bar{t} > 0$, the initial time interval until the time instant at which one out of the two conditions is verified:

(1) $n_1(\bar{t}) = \bar{n}_1$ and $n_3(\bar{t}) < \bar{n}_3$;
(2) $n_1(\bar{t}) < \bar{n}_1$ and $n_3(\bar{t}) = \bar{n}_3$.

Note that the condition $n_1(\bar{t}) = \bar{n}_1$, $n_3(\bar{t}) = \bar{n}_3$ can be excluded starting from a point different from E_2 because of the local instability of E_2. If the first condition were reached in $\bar{t}$ then the tumour would indefinitely grow for $t > \bar{t}$, while if the second one were satisfied then the tumour would be eradicated.

Fig. 5 shows an example of state trajectories obtained changing the initial tumour size n_{10} and choosing the model parameters such that relations (7) are satisfied. In particular, model parameters and administration rate are chosen as in Fig. 2 (see Section 2) while n_{10} is set in the interval $(0, 2\bar{n}_1]$. Note that, for this realistic case (mouse
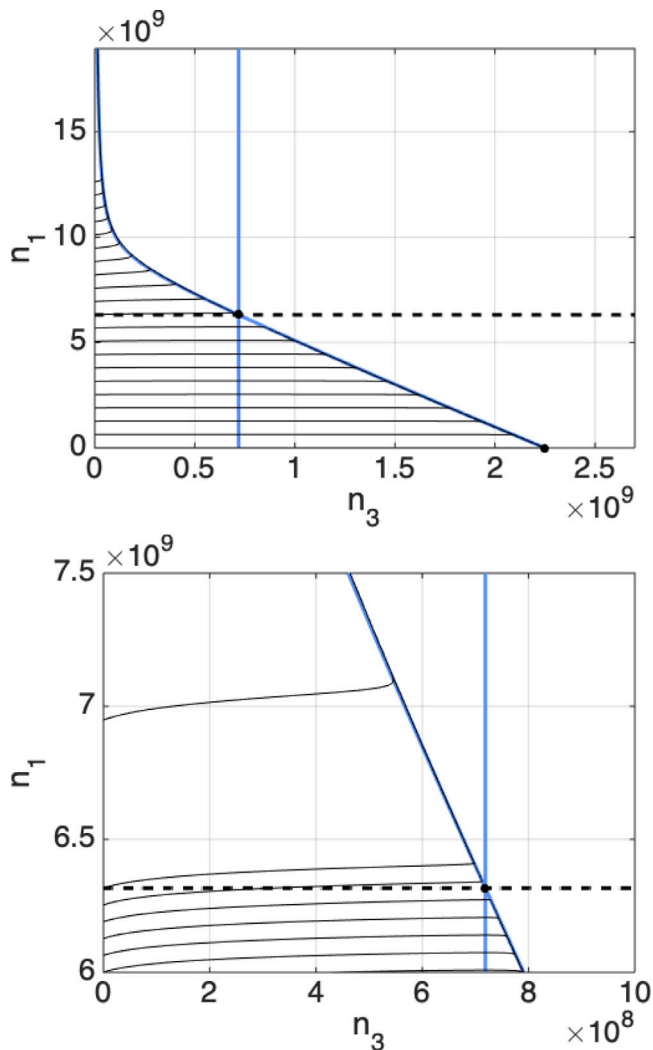
Fig. 5. State trajectories for $n_{10} \in (0, 2\bar{n}_1]$; model parameters taken from Table 2 and administration rate $\bar{r} = 1.53 \cdot 10^9$; critical values: $\bar{n}_3 = 7.1864 \cdot 10^8$, $\bar{n}_1 = 6.3168 \cdot 10^9$, obtained from Eqs. (9), (16). Panel A: The trajectories start from 20 equispaced values of n_{10} in the interval $(0, 2\bar{n}_1]$. Panel B: Increased number of initial points; the sampling interval of n_{10} is reduced by ten times in $(0, \bar{n}_1]$.

breast cancer cells and Pegylated Liposomal Doxorubicin treatment), once $\bar{r}$ is fixed ($1.53 \cdot 10^9$ drug molecules per day), the transition from stability to instability is obtained when n_{10} is very close to the threshold $\bar{n}_1$, that is when n_{10} is over the 98% of $\bar{n}_1$.

The remark given above shows the importance of suitably choosing the therapy intensity based on the tumour size. In particular, dealing with a constant therapy, the evaluation of the initial size has been proved to be crucial. More in general, dealing with variable administration rates, some information on the current size of the tumour is necessary to adequately tune the therapy. As shown in the next section, a control law which automatically adjusts the administration rate based on some evaluation of the tumour evolution can actually obtain the tumour eradication.

4. Model dynamics under a suitable state-feedback control law

In the previous section, an analysis of possible tumour eradication has been performed by means of a constant therapy administration, which has the advantage that it is only dependent on the system parameters, without exploiting any real-time information about the system dynamics.

However, as shown in the final part of the previous Section and illustrated by Fig. 4, the constant therapy approach suffers the following important limitations:

1. big tumours having an initial size larger than or equal to the critical size n_{10}^{max} (see Eq. (17)) cannot be eradicated by an admissible constant therapy, i.e. using an administration rate s.t. $\bar{r} < \rho$;

2. there is no guarantee that tumours with an initial size smaller than n_{10}^{max} can be actually eradicated using a constant therapy; for such a case, condition 1 of Remark 1 is a necessary and sufficient condition for a successful therapy.

In the present section we design a suitable control law able to eradicate the tumour independently of its initial size (i.e. the tumour dimension at the therapy planning) provided that some real-time information on the dynamical evolution of the tumour can be inferred. In the following, we focus on the autonomous subsystem $z = (n_1, n_3)^T$, described by the first and third equation of the ODE system (3), and we restrict our analysis to the meaningful case given by Eq. (7), which, in the presence of a constant therapy $r(t) = \bar{r}$, is characterized by a locally asymptotically stable equilibrium $z^e = (0, \bar{\bar{n}}_3)^T$, with $\bar{\bar{n}}_3 = M_4 \frac{\bar{r}}{\rho - \bar{r}}$, and by a stability region depicted by the green area of Fig. 4.

4.1. The tumour model is not stabilizable at the origin

In this subsection we prove that a non-zero therapy is necessary to eradicate the tumour reaching a stable equilibrium, so there exist no feedback laws able to stabilize the tumour by means of an asymptotically vanishing therapy rate.

We start noticing that the linearization of the reduced (autonomous) dynamics $z = (n_1, n_3)$ of Eq. (3) around the origin leads to

$$\dot{z}(t) \simeq Az(t) + Br(t), \tag{18}$$

with $A = \begin{bmatrix} (k_1 - k_2) & 0 \\ 0 & -\frac{\rho}{M_4} \end{bmatrix}$, $B = \begin{bmatrix} 0 \\ 1 \end{bmatrix}$. So the origin is a saddle (unstable equilibrium) of the uncontrolled system, because of the positive eigenvalue $\lambda_1 = k_1 - k_2$.

To show that neither linear nor nonlinear feedback laws can stabilize the system, it is sufficient (see Sastry, 2013, Chapter 6) to run the PBH test of stabilizability on the positive eigenvalue λ_1 of the linearized system:

Stabilizability of the origin $\iff rank\left(\begin{bmatrix} A - \lambda_1 I & B \end{bmatrix}\right) = dim(A).$ (19)

In our case, we get

$$rank(\begin{bmatrix} A - \lambda_1 I & B \end{bmatrix}) = rank\left(\begin{bmatrix} 0 & 0 & 0 \\ 0 & -\frac{\rho}{M_4} - (k_1 - k_2) & 1 \end{bmatrix}\right) = 1 < 2.$$

(20)

The test fails, implying that the n_1 dynamics cannot be stabilized in a neighbourhood of the origin. This is in perfect agreement with Fig. 4 and with the sign of $\dot{n}_1$ with $n_1 > 0$ (see Eqs. (8)–(9)):

$$\dot{n}_1|_{n_1 > 0} \geq 0 \iff (k_1 - k_2) - k_5 \frac{n_3}{M_5 + n_3} \geq 0 \iff n_3 \in [0, \bar{n}_3] \tag{21}$$

so for n_3 lower than $\bar{n}_3$, the tumour volume cannot decrease, independently of the nature of the therapy, since the input term r does not directly affect the n_1 dynamics.

From the previous discussion, we can conclude that feedback cannot help in avoiding the problem that the therapy must be constantly administered to prevent a new tumour wave.
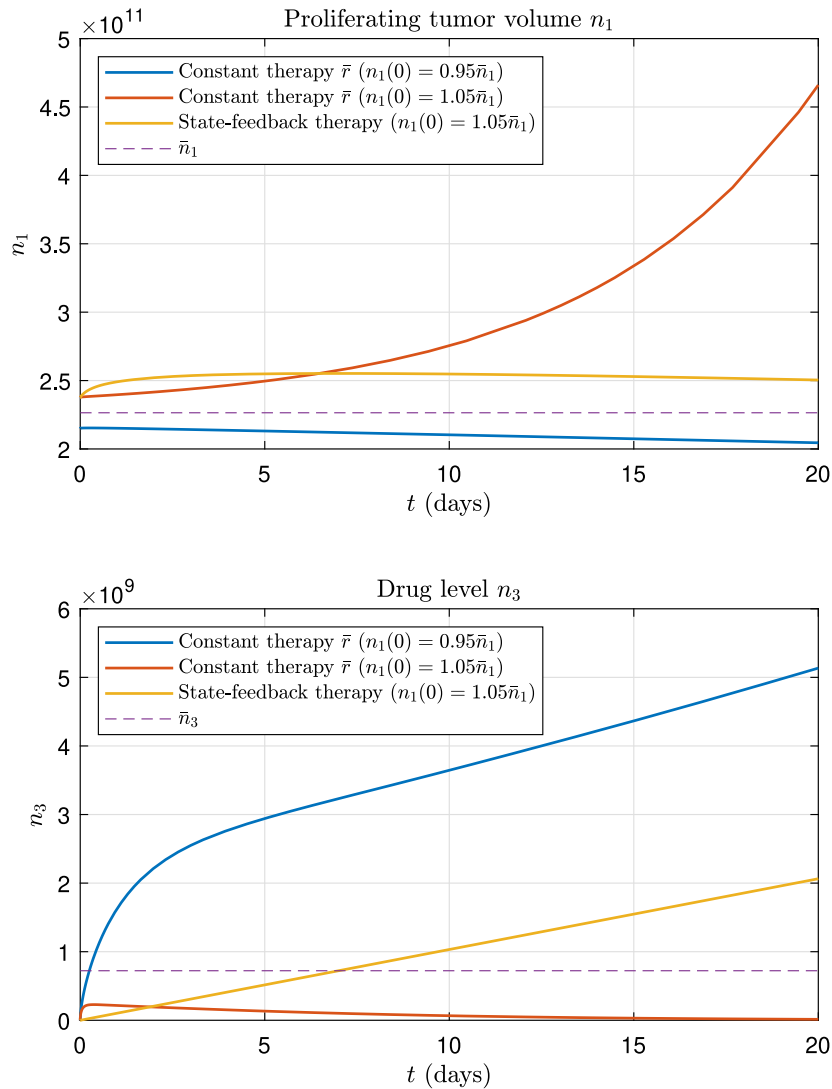
Fig. 6. Comparison between constant therapy regime and state feedback in the short term (20 days): tumour level n_1 (top panel) and drug level n_3 (bottom panel). Simulations are run from different values of the initial tumour level: $n_1(0) = 0.95\bar{n}_1$ (for constant therapy, blue line) and $n_1(0) = 1.05\bar{n}_1$ (for constant therapy, red line, and state-feedback therapy, yellow line); the constant therapy rate and the initial conditions for dead tumour cells and drug level are kept constant at the values $\bar{r} = 0.95\rho$, $n_2(0) = 100$ and $n(3) = 0$, respectively. Parameters are taken from Table 2.

4.2. Feedback laws can eradicate arbitrarily large tumours

The limitations about the constant therapy evidenced above come from the necessity of making a permanent choice on the size of the constant administration rate at the beginning of the therapy, exploiting at most an evaluation of the initial tumour size. In the following, we show that a feedback control is actually able to overcome such limitations allowing to eradicate the tumour even when only partial information about the system dynamics are available. Each drug delivery regimen starts with the initial condition for the treatment $n_3(0) = 0$, so no therapy was administered so far.

As shown in the proof of Theorem 1, large tumours belonging to the n_1 axis within the red zone of Fig. 4 (characterized by $\dot{n}_1 > 0$), i.e. tumours with an initial dimension n_1 higher than $\bar{n}_1$, cannot be eradicated by constant therapy, since the drug level dynamics n_3 cannot reach the zone $n_3 > \bar{n}_3$ (characterized by $\dot{n}_1 < 0$) without crossing before the curve $n_1 = g(n_3)$, beyond which $\dot{n}_3 < 0$ (n_3 decreases). In a nutshell, the tumour is so big that an admissible (lower than ρ) constant administration rate cannot accumulate up to a sufficient drug level to undermine the tumour volume.

The situation is different if we are able to tune the therapy in real-time depending on the estimated tumour volume. To this end, we assume that a conservative estimate of the state variables is available, i.e. $\hat{n}_1(t) \geq n_1(t)$, $\hat{n}_3(t) \geq n_3(t)$. The strategy can be divided into different steps.

Step 1. Guarantee drug level accumulation. As a matter of fact, differently from constant therapy, when the administration rate is changed over time based on the state estimation, we can always guarantee an increase of the drug level, independently of the tumour size. In fact, based on the conservative state estimates $\hat{n}_1$, $\hat{n}_3$ given above, the n_3 dynamics implies that

$$\dot{n}_3(t) = -\rho \frac{n_3(t)}{M_4 + n_3(t)} - k_5 n_1(t) \frac{n_3(t)}{M_5 + n_3(t)} + r(t)$$
$$\geq -\rho \frac{\hat{n}_3(t)}{M_4 + \hat{n}_3(t)} - k_5 \hat{n}_1(t) \frac{\hat{n}_3(t)}{M_5 + \hat{n}_3(t)} + r(t) \qquad (22)$$

due to the fact that the Michaelis–Menten function is increasing. So we have the following implication:

$$r(t) > r_{LB}(t) := \rho \frac{\hat{n}_3(t)}{M_4 + \hat{n}_3(t)} + k_5 \hat{n}_1(t) \frac{\hat{n}_3(t)}{M_5 + \hat{n}_3(t)} \implies \dot{n}_3(t) > 0, \qquad (23)$$
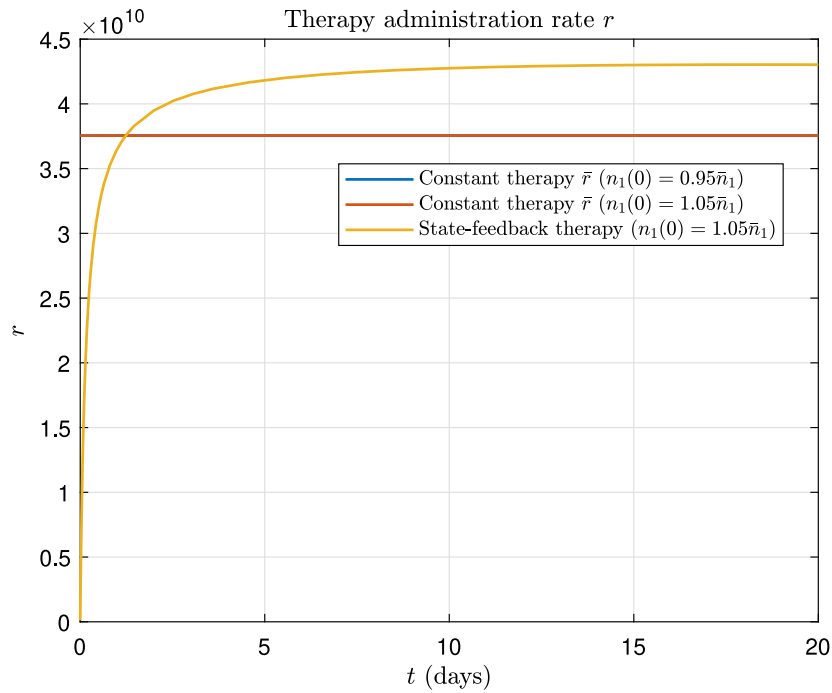
Fig. 7. Comparison between constant therapy regime and state feedback in the short term (20 days): administered therapy r. Simulations are run from different values of the initial tumour level: $n_1(0) = 0.95\bar{n}_1$ (for constant therapy, blue line) and $n_1(0) = 1.05\bar{n}_1$ (for constant therapy, red line, and state-feedback therapy, yellow line); the constant therapy rate and the initial conditions for dead tumour cells and drug level are kept constant at the values $\bar{r} = 0.95\rho$, $n_2(0) = 100$ and $n(3) = 0$, respectively. Parameters are taken from Table 2.
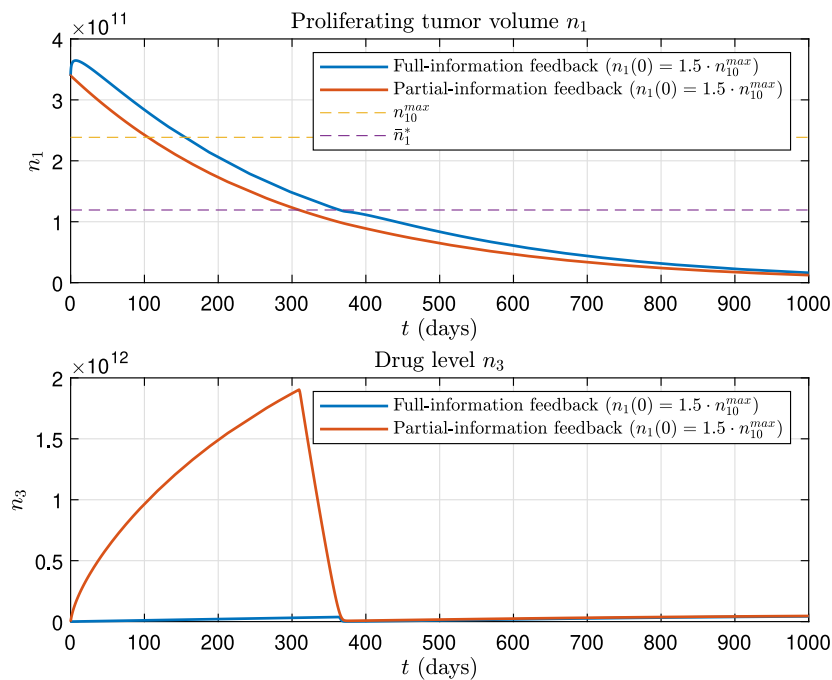

Fig. 8. Comparison between full information and partial information feedback laws in the long term (1000 days): tumour level n_1 (top panel) and drug level n_3 (bottom panel). Simulations are run from the initial state $(n_1(0), n_2(0), n_3(0)) = (1.5 \cdot n_{10}^{max}, 100, 0)$, with parameters taken from Table 2. The time $\bar{t}_2$ required to switch to a constant therapy $\bar{r}^* = \frac{(1+\beta)\rho}{2}$ is lower ($\bar{t}_2 = 326$) in the case of imperfect information with respect to full state feedback ($\bar{t}_2 = 380$).

Fig. 9. Comparison between full information and partial information feedback laws in the long term (1000 days): administered therapy r. Simulations are run from the initial state $(n_1(0), n_2(0), n_3(0)) = (1.5 \cdot n_{10}^{max}, 100, 0)$, with parameters taken from Table 2. The time $\bar{t}_2$ required to switch to a constant therapy $\bar{r}^* = \frac{(1+\beta)\rho}{2}$ is lower ($\bar{t}_2 = 326$) in the case of imperfect information with respect to full state feedback ($\bar{t}_2 = 380$).
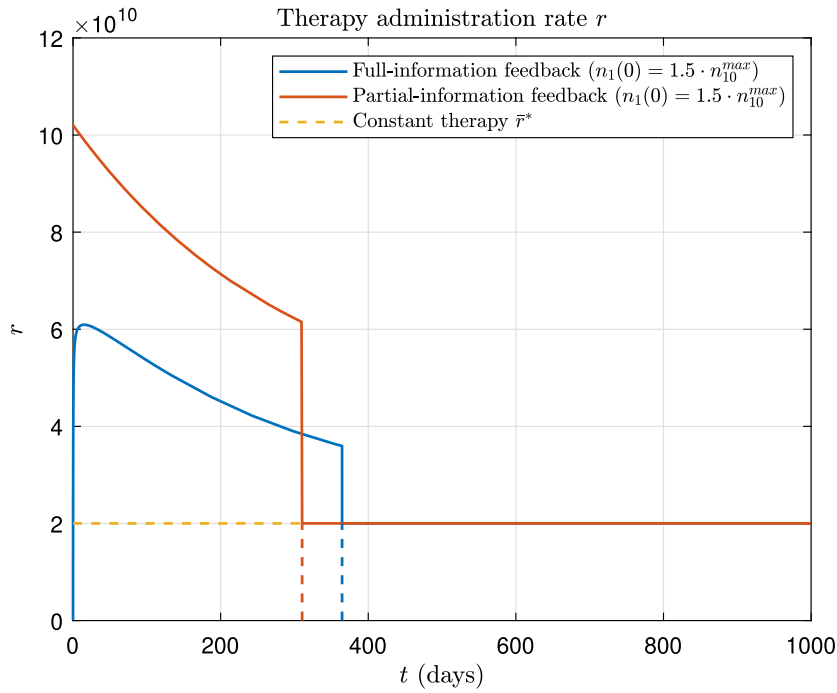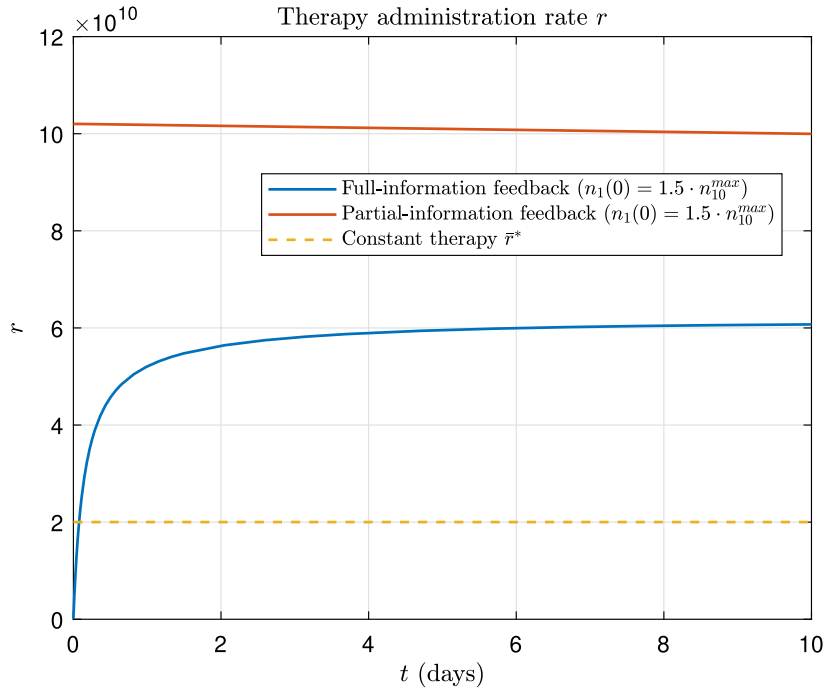

Fig. 10. Comparison between full information and partial information feedback laws in the short term (10 days): administered therapy r. Simulations are run from the initial state $(n_1(0), n_2(0), n_3(0)) = (1.5 \cdot n_{10}^{max}, 100, 0)$, with parameters taken from Table 2.

where $r_{LB}(t)$ is a lower bound for the administration rate $r(t)$ evaluated on the basis of the state estimate.

If we have no information about the drug therapy accumulation, but the tumour estimation is still available, due to the fact that the Michaelis–Menten function takes value in $[0, 1)$ we can further elaborate the bound (22) to obtain:

$$\dot{n}_3(t) \geq -\rho \frac{\hat{n}_3(t)}{M_4 + \hat{n}_3(t)} - k_5 \hat{n}_1(t) \frac{\hat{n}_3(t)}{M_5 + \hat{n}_3(t)} + r(t)$$

$$> -\rho - k_5 \hat{n}_1(t) + r(t). \tag{24}$$

A higher lower-bound for $r(t)$, only dependent on $\hat{n}_1$, is then obtained to guarantee $\dot{n}_3 > 0$:

$$r(t) > r_{LB}(t) := \rho + k_5 \hat{n}_1(t) \implies \dot{n}_3(t) > 0. \tag{25}$$

The previous Eqs. (23) and (25) provide conservative lower bounds for the administration rate ensuring the drug level accumulation, so
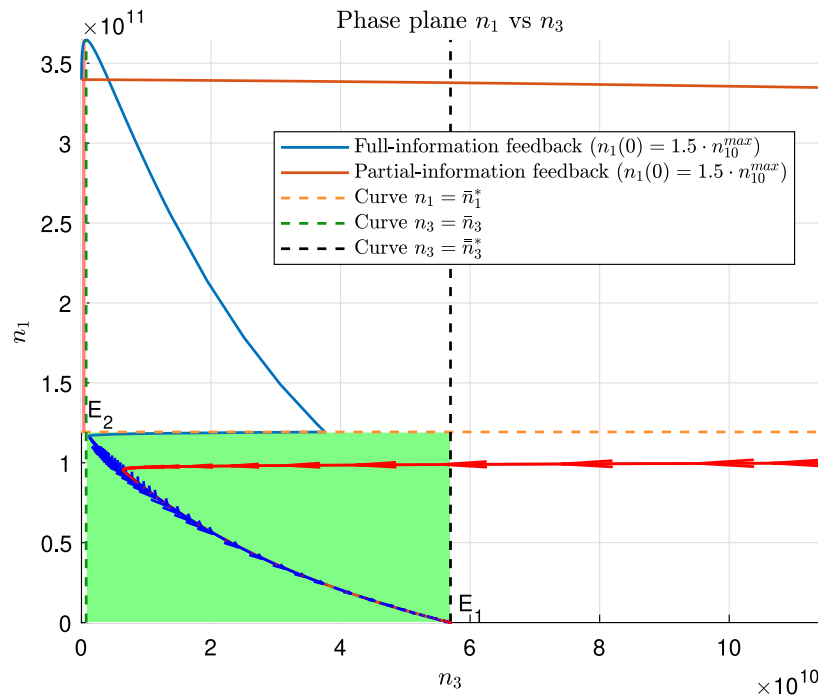
Fig. 11. Comparison between full information and partial information feedback laws in the very long term (5000 days): phase plot n_1 vs. n_3. Simulations are run from the initial state $(n_1(0), n_2(0), n_3(0)) = (1.5 \cdot n_{10}^{max}, 100, 0)$, with parameters taken from Table 2.

that the zone $n_3 > \bar{n}_3$ can be reached in a finite time. For example, the condition $n_3(t) > \bar{n}_3$ for $t \geq \bar{t}_1$ can be guaranteed for any desired $\bar{t}_1$ provided that $r(t)$ is chosen as

$$r(t) = r_{LB}(t) + \frac{\bar{n}_3}{\bar{t}_1} \tag{26}$$

and the lower bound $r_{LB}(t)$ is set according to Eq. (25). In fact, by integrating $\dot{n}_3$ and exploiting Eqs. (24), (25), (26), when $t \geq \bar{t}_1$ we get

$$
\begin{aligned}
n_3(t) &= n_3(0) + \int_0^t \dot{n}_3(\tau) d\tau \\
&> \int_0^t \left(-\rho - k_5 \hat{n}_1(\tau) + r(\tau) \right) d\tau \\
&= \int_0^t \left(-\rho - k_5 \hat{n}_1(\tau) + r_{LB}(\tau) + \frac{\bar{n}_3}{\bar{t}_1} \right) d\tau \\
&= \int_0^t \left(\frac{\bar{n}_3}{\bar{t}_1} \right) d\tau = \frac{\bar{n}_3}{\bar{t}_1} t \geq \frac{\bar{n}_3}{\bar{t}_1} \bar{t}_1 = \bar{n}_3,
\end{aligned}
$$

which is the desired condition on the derivative of n_3.

Notice that the therapy lower bounds (23) and (25) are possibly increasing in this first phase, since n_1 and n_3 are actually increasing with time until the drug threshold $\bar{n}_3$ is reached. We also note that the value of ρ, limiting the size of the constant administration rate, is no more a boundary for a time-varying administration. In fact, since the feedback control can be applied for finite time intervals, $r(t)$ can exceed the value of ρ, as in Eq. (25), without risking an unlimited accumulation of drug.

Step 2. Guarantee tumour reduction. In the previous step we proved that the control action $r(t)$ ensures drug accumulation for any tumour size. It is now possible to keep the same control input of Step 1 (this is the simple choice we adopt in the following numerical simulations) or to switch to a possibly milder therapy guaranteeing $\dot{n}_3 \geq 0$ (and not strictly $\dot{n}_3 > 0$), so that $n_3(t) > \bar{n}_3$ is guaranteed for any $t \geq \bar{t}_1$, namely the drug concentration of the controlled system cannot decrease below the threshold $\bar{n}_3$ from $\bar{t}_1$ on. This guarantees that $\dot{n}_1 < 0$ since time $\bar{t}_1$, i.e. the tumour size is actually shrinking from $\bar{t}_1$ on and that the decreasing behaviour is surely maintained under the proposed control action, in agreement with Eq. (8) and Fig. 4.

Step 3. Switch to constant therapy and long-term tumour removal. In the previous steps we provided the formulation of a therapy ensuring $\dot{n}_3 > 0$, as well as $\dot{n}_1 < 0$ from a given instant $\bar{t}_1$ onwards. However, it is not recommended the consequent drug accumulation to be maintained for indefinitely long periods, but the control action should switch to a lower (possibly constant) administration rate as soon as favourable conditions regarding tumour eradication are reached.

To this end, we first need to identify a suitable constant administration rate $\bar{r} = \bar{r}^*$ in the admissibility interval $(\beta\rho, \rho)$. This choice could be a compromise between patient safety (keeping $\bar{r}^*$ far from ρ) and eradication rapidity (rising for increasing $\bar{r}^*$). After choosing the desired $\bar{r}^*$, the corresponding value $\bar{n}_1^*$ is uniquely determined according to Eq. (16), i.e. $\bar{n}_1^* = \frac{\bar{r}^* - \beta\rho}{k_1 - k_2}$. Such a value gives a threshold for the tumour shrinking and allows to identify the time instant $\bar{t}_2$ at which the switching from the feedback control law to the constant administration rate can be performed, by virtue of the property $n_1(\bar{t}_2) \leq \bar{n}_1^*$.

More formally, the control action $r(t)$ is switched to $r(t) = \bar{r}^*$ for $t \geq \bar{t}_2$, where $\bar{t}_2$ can be determined by the simple condition $n_1(\bar{t}_2) = \bar{n}_1^*$. Notice that, in absence of accurate real-time information or late detection of the condition $n_1(t) \leq \bar{n}_1^*$, a conservative evaluation of time $\bar{t}_2$ can be used, i.e. a time larger than the real crossing time. This postpones the switching to the constant therapy regime but the delay is acceptable, since the proposed control law guarantees $n_3(t) > \bar{n}_3$ and $\dot{n}_1(t) < 0$ since $\bar{t}_1$ by construction.

Conditions $n_1(t) \leq \bar{n}_1^*$ and $n_3(t) > \bar{n}_3$ guaranteed for $t \geq \bar{t}_2$ finally ensure that the dynamics has reached the green zone of Fig. 4 within time $\bar{t}_2$ (where the general $\bar{n}_1$ of the picture is now $\bar{n}_1^*$). Since the therapy $r(t)$ is switched to constant therapy $r(t) = \bar{r}^*$ for $t \geq \bar{t}_2$, the derivative signs shown in Fig. 4 and discussed in the previous section are valid. In particular, it can be readily shown that the green region $G = \{z = (n_1, n_3) : n_1 < \bar{n}_1 \ \& \ n_3 > \bar{n}_3\}$ of Fig. 4 is a basin of attraction for the equilibrium z^e (E_1 in the figure). This can be verified by means of the Lyapunov function (see e.g. Khalil, 1996) $V(z) = \frac{1}{2}(z - z^e)^T(z - z^e)$, whose derivative along the system trajectories is $\dot{V} = (z - z^e)^T \dot{z} = n_1 \dot{n}_1 + (n_3 - \bar{n}_3)\dot{n}_3 < 0$ in $G \setminus \{z^e\}$. This ensures the asymptotic convergence to the tumour-free equilibrium.

4.3. Simulation results

Numerical simulations have been performed in MATLAB®. In all the simulations, the initial conditions for dead tumour cells and drug level are kept constant at the values $n_2(0) = 100$ and $n(3) = 0$, respectively, while different values of the initial tumour level $n_1(0)$ are considered.

Figs. 6–7 show the effect of constant therapy compared with state feedback using full information. These simulations compare the evolution with the same admissible constant therapy $\bar{r} = 0.95\rho \in (\beta\rho, \rho)$ for two different values of $n_1(0)$, equal to $0.95\bar{n}_1$ and to $1.05\bar{n}_1$, respectively. In a short term horizon (20 days), it is shown (Fig. 6, top panel) that a constant therapy is not able to contrast tumours with size larger than $\bar{n}_1$, differently from the state feedback computed according to (26), with $\bar{\iota}_1 = 7$ (days), and the lower bound in (23), with $n_1(0) = 1.05\bar{n}_1$, $\hat{n}_1(t) = n_1(t)$ and $\hat{n}_3(t) = n_3(t)$ (perfect information). In the latter case, the state feedback after a time interval of $\bar{\iota}_1$ days is able to start (slowly) the tumour reduction. The different behaviour of n_1 in the different cases produces dissimilar trajectories for the coupled variable n_3 (drug level, Fig. 6, bottom panel). Fig. 7 shows that the administered therapy is comparable in the constant and in the feedback case.

Figs. 8–9 instead show a comparison, over a long time horizon (1000 days), between the state feedback (26) with full information, that is $\hat{n}_1(t) = n_1(t)$, $\hat{n}_3(t) = n_3(t)$, and with the smaller lower bound (23) (the same formula adopted in the short-term simulation described above), and the feedback law (26) with partial and inaccurate state information, i.e. $\hat{n}_1(t) > n_1(t)$ and no estimation of $n_3(t)$, and with the higher lower bound (25). In particular, in the latter case the available imperfect information about the current tumour size is given by $\hat{n}_1(t) = 1.1n_1(t)$ at all times. The initial tumour level has been set to $n_1(0) = 1.5 \cdot n_{10}^{max}$, with n_{10}^{max} defined in (17). The partial information feedback, due to the tumour size overestimation and the more conservative lower bound, forces a faster tumour decrease (Fig. 8, top panel), thanks to a higher drug level (Fig. 8, bottom panel), as a consequence of a larger quantity of administered drug (Fig. 9) in the transient with respect to full state feedback. As illustrated in the previous part, in the control procedure it is required to choose a constant therapy level $\bar{r} = \bar{r}^*$ in the admissibility interval $(\beta\rho, \rho)$; to this end, we set the steady-state therapy equal to the midpoint $\bar{r}^* = \frac{(1+\beta)\rho}{2}$ of such an interval, which is a robust choice with respect to possible model parameter uncertainties. According to Eq. (16), $\bar{r} = \bar{r}^*$ determines the value of $\bar{n}_1 = \bar{n}_1^*$ to be reached before switching (at time $\bar{\iota}_2$) to the constant therapy regime, i.e. $n_1(t) \le \bar{n}_1^*$ for $t \ge \bar{\iota}_2$. As a consequence of the higher drug administered in the transient, the time $\bar{\iota}_2$ required to switch to a constant therapy is lower ($\bar{\iota}_2 = 326$) in the case of imperfect information (see Fig. 9) with respect to full state feedback ($\bar{\iota}_2 = 380$). Fig. 10 shows a zoom of Fig. 9 limited to the first 10 days, which allows to better observe the initial rise of the full-information feedback law. Finally, Fig. 11 shows (over an even larger horizon of 5000 days) the asymptotic convergence of the (n_3, n_1) dynamics in the phase plane to the controlled equilibrium $E_1 = \left(0, 0, \bar{n}_3^*\right)$, with $\bar{n}_3^* = M_4 \frac{\bar{r}^*}{\rho - \bar{r}^*}$, consistently with Fig. 4.

5. Conclusions

This paper addresses the problem of tumour growth control exploiting a minimally parameterized and low-dimensional deterministic ODE model of tumour growth under treatment, which is able to provide a good approximation of the first-order moment of the more realistic stochastic formulation. Two alternative control approaches are here investigated. The first one is based on a constant infusion of drug, while the second one proposes a state-feedback control scheme, exploiting partial or complete knowledge of the state.

The results of the paper show that a constant therapy, initially set and never adjusted during time, has several limitations. In particular, the initial tumour size is responsible for the possible therapy failure and too large tumours have no chances to be eradicated by admissible (i.e. tolerable) constant infusions. Conversely, the proposed state-feedback control is very promising since it is always able to eradicate arbitrarily large tumours.

We finally highlight that the deterministic modelling framework used for the present analysis suffers from an intrinsic limitation; indeed, since the tumour dynamics is linear with respect to tumour size, the tumour can be eradicated only asymptotically, i.e. over an infinite time horizon. Preliminary studies on the discrete stochastic framework instead show that, with the same conditions on the model parameters, the tumour can be eradicated with probability 1 in finite time. Therefore, the design of a stochastic control is a future perspective naturally arising from the results obtained in this paper.

CRediT authorship contribution statement

Federico Papa: Conceptualization, Methodology, Software, Writing – original draft, Writing – review & editing, Formal analysis, Investigation, Supervision. **Alessandro Borri:** Conceptualization, Methodology, Software, Writing – original draft, Writing – review & editing, Formal analysis, Investigation, Supervision. **Pasquale Palumbo:** Conceptualization, Methodology, Writing – original draft, Writing – review & editing, Formal analysis, Investigation, Supervision, Project administration.

Declaration of competing interest

The authors declare that they have no known competing financial interests or personal relationships that could have appeared to influence the work reported in this paper.

Appendix. Numerical integration

The ODE model describing the approximated average value solutions of the CME is integrated according to the standard `ode45` MATLAB Runge–Kutta function.

In order to generate random paths from the CME model, we exploited the τ-leap algorithm (Gillespie, 2001), an approximate procedure of the statistically exact Gillespie algorithm Gillespie (1976). Indeed, the standard Gillespie algorithm involves a prohibitively long computer time if the molecular populations of at least some of the reactant species are very large, and the present stochastic model actually may involve millions of tumour cells: in all these cases, the τ-leap approximation is the usual trade-off that overcomes Gillespie bottlenecks Gillespie (2001). It is based on a fixed sampling time τ, according to which, for any time instant $t_k = k\tau$, we assume that the propensity a_i of each reaction i ($i = 1, \ldots, M$) is constant within the time interval $[t_k, t_{k+1}]$ of duration τ, and equal to the propensity value at the beginning of the sampling interval $a_i(n(t_k))$; therefore we approximate the number l of occurrences of any reaction R_i as a Poisson random variable of parameter $\lambda = a_i(n(t_k))\tau$:

$$P\big(n(t_k + \tau) - n(t_k) = l\delta_i\big) \simeq \frac{\big(a_i(n(t_k))\tau\big)^l \cdot e^{-a_i(n(t_k))\tau}}{l!}, \tag{A.1}$$

where δ_i is the reset associated to reaction i, namely reaction i transforms a state vector n into the state vector $n + \delta_i$.

Therefore, by accounting for all the reactions $i = 1, \ldots, M$, one gets the following approximate discrete-time evolution for the process:

$$n(t_{k+1}) = n(t_k) + \sum_{i=1}^{M} \delta_i \Lambda_i(t), \qquad k = 0, 1, \ldots, \tag{A.2}$$

where $\Lambda_i(t_k)$ is a Poisson random variable of parameter $a_i(n(t_k))\tau$.

References

Borri, A., Carravetta, F., Mavelli, G., Palumbo, P., 2016. Block-tridiagonal state-space realization of Chemical Master Equations: A tool to compute explicit solutions. J. Comput. Appl. Math. 296, 410–426.

Borri, A., Palumbo, P., Papa, F., 2020. Deterministic vs stochastic formulations and qualitative analysis of a recent tumour growth model. IFAC-PapersOnLine 53 (2), 16418–16423. http://dx.doi.org/10.1016/j.ifacol.2020.12.724.

Cacace, F., Cusimano, V., Germani, A., Palumbo, P., 2018a. Optimal impulsive control with application to antiangiogenic tumor therapy. IEEE Trans. Control Syst. Technol. 1–12.

Cacace, F., Cusimano, V., Germani, A., Palumbo, P., Papa, F., 2018b. Closed-loop control of tumor growth by means of anti-angiogenic administration. Math. Biosci. Eng. 15 (4).

d'Onofrio, A., Gandolfi, A., 2004. Tumour eradication by antiangiogenic therapy: Analysis and extensions of the model by Hahnfeldt et al. (1999). Math. Biosci. 191, 159–184.

d'Onofrio, A., Gandolfi, A., 2010. Chemotherapy of vascularised tumours: Role of vessel density and the effect of vascular "pruning". J. Theoret. Biol. 264, 253–265.

d'Onofrio, A., Ledzewicz, U., Maurer, H., Schättler, H., 2009. On optimal delivery of combination therapy for tumors. Math. Biosci. 222 (1), 13–26.

Drexler, D.A., Ferenci, T., Lovrics, A., Kovács, L., 2019. Modeling of tumor growth incorporating the effect of pegylated liposomal doxorubicin. In: IEEE 23rd Int. Conf. on Intelligent Engineering Systems. pp. 369–374.

Drexler, D.A., Sápi, J., Kovács, L., 2017a. A minimal model of tumor growth with angiogenic inhibition using bevacizumab. In: Proceedings of the 2017 IEEE 15th International Symposium on Applied Machine Intelligence and Informatics. pp. 185–190.

Drexler, D.A., Sápi, J., Kovács, L., 2017b. Modeling of tumor growth incorporating the effects of necrosis and the effect of bevacizumab. Complexity 1–11.

Drexler, D., Sápi, J., Kovács, L., 2017c. Optimal discrete time control of antiangiogenic tumor therapy. In: Proc. 20th IFAC World Congress. pp. 14046–14051.

Dzyubak, L., Dzyubak, O., Awrejcewicz, J., 2019. Controlling and stabilizing unpredictable behavior of metabolic reactions and carcinogenesis in biological systems. Nonlinear Dynam. 97, 1853–1866.

Feinberg, M., 2019. Foundations of Chemical Reaction Network Theory. In: Applied Mathematical Sciences, Springer.

Gillespie, D.T., 1976. A general method for numerically simulating the stochastic time evolution of coupled chemical reactions. J. Comput. Phys. 22, 403–434.

Gillespie, D.T., 2001. Approximate accelerated stochastic simulation of chemically reacting systems. J. Chem. Phys. 115, 1716–1733.

Hahnfeldt, P., Panigrahy, D., Folkman, J., Hlatky, L., 1999. Tumor development under angiogenic signaling. Cancer Res. 59 (19), 4770–4775.

van Kampen, N.G., 2007. Stochastic Processes in Physics and Chemistry, third ed. Elsevier, The Nederlands.

Khalil, H., 1996. Nonlinear systems, third ed. Prentice Hall, New Jersey.

Ledzewicz, U., Maurer, H., Schaettler, H., 2011. Optimal and suboptimal protocols for a mathematical model for tumor anti-angiogenesis in combination with chemotherapy. Math. Biosci. Eng. 8 (2), 307–323.

Ledzewicz, U., Schättler, H., 2008. Optimal and suboptimal protocols for a class of mathematical models of tumor anti-angiogenesis. J. Theoret. Biol. 252 (2), 295–312.

Liu, Z., Guo, C., Li, H., Zhao, L., 2019. Analysis of a nonlinear age-structured tumor cell population model. Nonlinear Dynam. 98, 283–300.

Medaglia, A., Colelli, G., Farina, L., Bacila, A., Bini, P., Marchioni, E., Figini, S., Pichiecchio, A., Zanella, M., 2022. Uncertainty quantification and control of kinetic models of tumour growth under clinical uncertainties. Int. J. Non-Linear Mech. 141, 103933. http://dx.doi.org/10.1016/j.ijnonlinmec.2022.103933.

Pinho, S., Bacelar, F., Andrade, R., Freedman, H., 2013. A mathematical model for the effect of anti-angiogenic therapy in the treatment of cancer tumours by chemotherapy. Nonlinear Anal. RWA 14 (1), 815–828. http://dx.doi.org/10.1016/j.nonrwa.2012.07.034.

Preziosi, L., Toscani, G., Zanella, M., 2021. Control of tumor growth distributions through kinetic methods. J. Theoret. Biol. 514, 110579. http://dx.doi.org/10.1016/j.jtbi.2021.110579.

Sápi, J., Drexler, D., Harmati, I., Sápi, Z., Kovács, L., 2016. Qualitative analysis of tumor growth model under antiangiogenic therapy–choosing the effective operating point and design parameters for controller design. Optim. Control Appl. Methods 37 (5), 848–866.

Sastry, S., 2013. Nonlinear Systems: Analysis, Stability, and Control. vol. 10, Springer Science & Business Media.

Wei, X., Cui, S., 2008. Existence and uniqueness of global solutions for a mathematical model of antiangiogenesis in tumor growth. Nonlinear Anal. RWA 9 (5), 1827–1836. http://dx.doi.org/10.1016/j.nonrwa.2007.05.013.